

AD-A256 587



October 8, 1992

Dr. George Yoder
Office of Naval Research
Code 1131
800 N. Quincy
Arlington VA 22217-5000

Dear Dr. Yoder: *George*

Enclosed please find a copy of the Annual Report for Grant #N0014-89-J-1708 "A Study of the Relationship Between Macroscopic Measures and Physical Processes Occurring During Crack Closure".

Should you have any questions or need further information, please do not hesitate to contact either myself or Dr. Stock.

Sincerely,

Steve

Stephen D. Antolovich
Professor of Materials Science and Engineering
Director, Mechanical Properties Research Lab.

DTIC
SELECTE
OCT 19 1992

DISTRIBUTION STATEMENT A
Approved for public release
Distribution Unlimited

92 1 110

Annual Report for

A Study of the Relationship Between Macroscopic Measures
and Physical Processes Occuring during Crack Closure

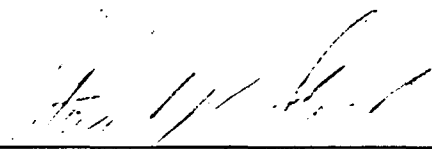
N0014-89-J-1708

submitted to:

Office of Naval Research
Attn. Dr. George Yoder
ONR Code 1131
800 N. Quincy
Arlington, Virginia 22217-5000

by


Stephen D. Antolovich
Mechanical Properties Res. Lab.
School of Materials Engineering
Georgia Institute of Technology
Atlanta, GA 30332-0245


Stuart R. Stock
Mechanical Properties Res. Lab.
School of Materials Engineering
Georgia Institute of Technology
Atlanta, GA 30332-0245

92 1 10 10

92-27297



TABLE OF CONTENTS

	Page
I. Physical Measurements of Crack Closure	1
II. Analytical Computations of the Effective Stress Intensity	4
III. Fractography and Fatigue Crack Propagation (FCP) Rates .	6
IV. Personnel	7
V. Interactions	8
VI. Presentations and Publications	9
VII. Awards	10
Table 1	12
Figures	13 - 28

Accession For	
NTIS GRA&I	<input checked="" type="checkbox"/>
DTIC TAB	<input type="checkbox"/>
Unannounced	<input type="checkbox"/>
Justification	
By <i>per ADA238423</i>	
Distribution/	
Availability Codes	
Dist	Avail and/or Special
<i>A-1</i>	

DTIC QUALITY INSPECTION REPORT

I. Physical Measurements of Crack Closure

Activity centered on the development and implementation of robust methods for measuring crack opening in the samples studied with X-ray Tomographic Microscopy (XTM). The existing XTM data of notched tensile (NT) samples consists of a three-dimensional stack of several hundred two-dimensional slices, each containing between 400x400 and 600x600 pixels. Analysis of the three-dimensional crack wandering through this volume is done in several steps. The first step is to determine the separation between crack faces using cuts perpendicular to the stack of slices (Figure 1). Separation will be measured as a function of position for the different applied loads. Cuts parallel to the load axis are expected to give a more precise measure of crack opening than measurements within planes parallel to the slices, especially when the openings are on the order of one or two pixels in size.

One way of easily following the variation of crack opening as a function of position in the sample is to project the amount of opening onto a single plane (Figure 2). This representation ignores the non-planarity of the crack, allows one to avoid the difficulties inherent in exactly registering images recorded at different load levels and produces higher precision in determining changes in crack openings for different loads. Many pixels along the crack plane are only partially occupied by the crack, and summing of partial volumes occurring along the load axis is necessary for accurate measurement of the total crack opening.

In calculating the partial volumes of pixels occupied by

cracks, it is crucial to define the precise attenuation of the matrix. Once this average is established, one needs to set a threshold value for the attenuation coefficient below which the voxel is considered to be occupied (partially) by a crack. On the one hand, this threshold must be close enough to the average so that crack opening is not significantly underestimated; and, on the other, it must be outside the noise in the reconstructed images so that automated crack measurement is robust. Typically, we have set the threshold by measuring the distribution of linear attenuation coefficients in a volume of the sample which did not contain the crack and by calculating the value of the absorption coefficient at a predetermined number of standard deviations below the average attenuation coefficient. Assuming that the attenuation of air is zero, the measured crack opening is the threshold value minus the value of pixel where crack is open.

Sample NT-4 was imaged with synchrotron XTM and had a 1.8 mm final diameter (initial diameter was 1.9 mm) after 34,760 cycles. This crack is quite short compared to that in NT-3 which was examined with laboratory XTM. Load levels up to the maximum load under which the crack propagated were examined. In the first series of data, the loads were 100, 80, 60, 40 and 20 lbs (45.4, 36.3, 27.2, 18.2 and 9.1 kg, respectively). A second series of XTM data was also collected at loads of 90, 70, 50, 30 and 10 lbs (40.9, 31.8, 22.7, 13.6 and 4.5 kg, respectively). The cuts intersecting the tip of the crack show an irregular crack front and a variable crack opening is calculated and mapped onto the nominal

crack plane (Figure 3). There are regions of closed or nearly closed cracks present far behind the crack tip, even at the maximum load level. Histograms of the measured crack openings show a significant decrease in crack opening from 45.4 kg (100 lbs) to 27.2 kg (60 lbs) and from 40.9 kg (90 lbs) to 22.7 kg (50 lbs) (Figure 4), but the shape of the histograms does not vary for the different loads. In this calculation, the threshold value is 90 to 92% of the average linear attenuation coefficient μ of Al-Li 2090, calculated from $> 10^4$ of pixels, and this corresponds to 0.6 standard deviations below the average attenuation coefficient.

Once "areas" of importance in the closure process are identified (i.e., positions where no changes in the opening are observed or where greatest changes are seen), we plan to examine the full three-dimensional data set quantitatively. This second step would focus on geometrical effects from the jagged crack, i.e., is the crack closing first at certain microstructural features such as the sides of ridges, etc. Three-dimensional renderings of the crack faces will be used to combine the complex crack geometry with the measured openings. The roughness of the crack, its nominal length and the presence of oxide particles can influence crack closure, and these aspects of microstructure will be examined carefully. These results will also be compared with SEM images of the crack face.

Discussions with Mr. R. Yancy of ARACOR, who operates the Air Force Materials Laboratory's medium resolution computed tomography apparatus, and with Air Force personnel have resulted in our group

being scheduled for time during summer 1992 in which to image the full compact tension samples under load. Also, continuing discussions with Dr. M. Barker of Lockheed Missiles and Space Corporation are anticipated to allow imaging at still higher resolution of reduced cross-section compact tension samples; this will probably be done during Fall 1992.

II. Analytical Computations of the Effective Stress Intensity Factors

In the previous report, an analytical expression for calculating the effective stress intensity factor using multiple asperities on the fracture surface was developed. It was considered to be an appropriate model to study realistic closure mechanisms. While closure is expected to occur mostly near the crack front, the number of asperities interfering with each other will be determined by the roughness dimension and the extent of mismatch. If 15 asperities of different roughness dimension are assumed to be arbitrarily distributed near the crack tip and groups of three far from the tip are eliminated one group at a time, the closure stress intensity factors for all six cases are shown in Figure 5. Note that the closure stress intensity factor for six asperities converges to that for higher number of asperities for closure loads larger than zero.

So far, all previous analytical crack closure models were made for a crack in an infinite medium. However the closure stress intensity factors may be quite different from those for a specimen

of finite dimension. Some correction factors, α and α_1 , were obtained for the influence functions in the calculation of stress intensity factor and COD under the internal pressure on the fracture surface. The correction factor, R_c , is defined as

$$R_c = \alpha\alpha_1 = K/K_{INF} = COD/COD_{INF} \quad , \quad (1)$$

where K_{INF} and COD_{INF} are the stress intensity factor and the crack opening displacement in an infinite medium, respectively. α and α_1 are the correction factors for semi-infinite and finite geometries, which are shown in Figure 6 and which are functions of a/b and c_i/a . Here, a , b , and c_i are the crack length, specimen width, and the distance from the center line of the pin hole to the applied load points. Their dimensions are shown in Figure 7. Table 1 shows comparisons of analytical α_1 values with finite element results. Three meshes with different crack lengths and contact points are shown in Figure 8. Figure 9 shows a plot of the correction factor, R_c , for different crack lengths (a/b) vs the contact point (c/a). Here, $c/a=1$ represents the crack tip location. From this, if contact occurs at $c/a=0.8$ for $a/b=0.68$ of the crack length, the stress intensity factor for the compact tension specimen will be 3.7 times larger than that for the infinite medium. In fact, some contacts at small c/a and large a/b were observed in Al-Li alloy crack propagation experiments. In this case the difference in the closure stress intensity factor will be quite large.

III. Fractography and Fatigue Crack Propagation (FCP) Rates

In the following sub-sections, experimental FCP data and fractographic observations are presented. This information provides a basis for correlating microscopic observations and macroscopic behavior with the analytical models.

FCP Testing of Al-Li Specimens

Three compact tension specimens mentioned in 1st annual report were tested for load ratios of $R=0.1$ and 0.7 . The FCP data (obtained according to ASTM E-647 specifications) are shown in Figure 10; FCP data previously obtained in this program is shown in Fig. 11, and the solid line shows good agreement with the crack propagation rates obtained using conventional compact tension samples (Yoder et al, 1988). The data trends appeared to be the same as those in other publications (Rao and Ritchie, 1991). In order to investigate the closure effect of the alloy, the closure stress intensity factors were calculated using conventional approaches, in which the closure load is determined from the intersection of two tangential lines drawn at maximum and minimum load points on the load-displacement curve. Figure 12 shows the degree of closure vs ΔK . Note that the closure occurred immediately upon crack initiation. When the parameter, ΔK_{eff} , accounting for the closure effect is used, the FCP rate is corrected as shown in Figure 13. The variation in data at early stages of crack growth is due to the thin specimen (≈ 0.08 inches), that yields less sensitivity in measuring potentials for the small amounts of crack

growth even if high currents (10 Amps) are applied.

B. Fractographic Analyses

The fracture surfaces of tested specimens were closely examined using SEM. When FCP rates are plotted against the crack length, the effect of closure is clear as shown in Figure 14. The FCP rate drops in the range of the crack length between 5.5 and 7.5mm, where large contact area were developed, instead of linearly increasing as the crack grows. The contact area is identified as the area in which an unusually large oxygen "peak" occurs in Auger spectroscopy. Micrographs (Figure 15 and 16) show the rough fracture surface, which is typical of this alloy; the fracture surface has the crystallographic features, and the change in fracture mode (illustrated by the dots in Figure 16) shows that the crack front was very irregular.

IV. Personnel

The following personnel have worked on the project

A. Principal Investigators

1. Stephen D. Antolovich Fracture Mechanics
analytical studies,
mechanical testing issues
2. Stuart R. Stock Tomography, radiography,
specimen design,
contacts with synchrotron
sources, design of rig,
mechanical testing issues

B. Students

1. Thomas Breunig Design of tensile rig,
mechanical testing,

tomography data acquisition

2. Abbas Guvenilir

Assistance with design of experiments, analysis of data, tomography data acquisition

3. Y. Jung

Finite element calculations of crack closure

V. Interactions

Interaction with other groups is important to the success of the project. The following interactions have been (or are being) established:

	<u>Organization</u>	<u>Person</u>	<u>Comments</u>
1.	Lawrence Livermore	John Kinney	A c t i v e collaboration software, laboratory and synchrotron x-ray tomographic microscopy
2.	Southwest Research Institute	David Davidson	Continuing discussion on closure
3.	CNAM (France)	C.Bathias	Discussions of closure in Al-Li alloys
4.	Stanford Synchrotron Radiation Laboratory	-	Proposal for beam time
5.	National Synchrotron	-	Proposal for beam time
6.	Cornell High Energy Synchrotron Source	-	Experiment performed

VI. Presentations and Publications (unless otherwise noted the presentation was given by S.R. Stock)

1. "A Portable Load Frame for in situ Computed Tomography of Monolithic and Composite Materials," (presented by T.M. Breunig), April/May 1991 ASTM E9.04 Meeting, Indianapolis.
2. "Damage in Metal Matrix Composites and Crack Face Interactions During in situ Loading of Al-Li Alloy 2090 Studied by X-ray Tomographic Microscopy," 1991 Industrial Computed Tomography II Topical Conference, American Society for Nondestructive Testing, May 1991, San Diego.
3. "X-ray Tomographic Microscopy of Sample Response During in situ and Interrupted Mechanical Testing," (poster), Pacific International Congress on X-ray Analytical Methods, August 1991, Honolulu.
4. "Crack Face Separation in the Interior of Al-Li 2090 Samples Quantified as a Function of Applied Load by in situ X-ray Tomographic Microscopy," (presented by A. Guvenilir) TMS-AIME Fall Meeting, October 1991, Cincinnati.
5. "X-ray Tomographic Microscopy and its Applications - Fatigue Crack Closure in Al-Li 2090, Damage Accumulation in SiC/Al and Chemical Vapor Infiltration Processing of Nicalon/SiC," Wright Laboratories (WL/MLLM), October 1991, Dayton.
6. "X-ray Tomographic Microscopy and its Applications: Fatigue Crack Closure in Al-Li 2090, Damage Accumulation in SiC/Al and Chemical Vapor Infiltration Processing of Nicalon/SiC," Quality Technology Division, General Electric Aircraft Engines, October 1991, Cincinnati.
7. "X-ray Tomographic Microscopy and its Applications in Fatigue Crack Closure and in Damage Accumulation in Composites," BP Research, October 1991, Cleveland.
8. T.M. Breunig, Y. Jung, S.R. Stock, J. Kinney and Stephen D. Antolovich: A Framework for Relating Macroscopic Measures and Physical Processes of Crack Closure Illustrated by a Study of Al-Li Alloy 2090. Presented at 22nd National Fracture Mechanics Symposium, June 28, 1990, Atlanta, Georgia. Fracture Mechanics: 22nd Symposium (Volume 1), ASTM STP 1131, H.A. Ernst, A. Saxena, and D.L. McDowell, Eds., American Society for Testing and Materials, 1992, pp. 749-761.

The final draft of one publication was being completed in February 1992 for publication in Materials Evaluation (the official journal

of the American Society for Nondestructive Testing). Its tentative title and authors are "A simple load frame for in situ computed tomography and x-ray tomographic microscopy," T. M. Breunig, S. R. Stock and R. C. Brown.

VII. Awards

T. M. Breunig and S.R. Stock, Georgia Institute of Technology, Co-recipients of an 1991 R&D 100 Award with Lawrence Livermore and Sandia-Livermore National Laboratories.

1. **ASME Nadai Award**, November, 1990. Award was granted by the American Society of Mechanical Engineers "for outstanding contributions toward understanding the relationships between microstructure, deformation mechanisms, fatigue and fracture in engineering alloys at high and low temperatures; for incorporating this understanding into the development of mechanical behavior and life prediction models, and for developing outstanding students in this and related areas".
2. Named as the first Honorary Professor (Professeur Invite') of the Conservatoire National des Arts et Metiers, Paris, France in 1989.

3. **Reaumur Medal of the French Metallurgical Society** in October 1988. This medal was awarded for "lifetime achievements in research having particular significance to industry". It is the top research award of the French Metallurgical Society.

4. **Elected Fellow of ASM International**, October 1987.

5. **Named as charter member of the Council of Fellows of ASM International** in January 1989.

Table 1. Comparison of Analytical α_1 Values with Finite Element Results.

a/b	0.36	0.44	0.52	0.60	0.68	0.76	0.84
α_1	1.085	1.088	1.049	1.008	0.982	0.975	0.980
FEM	-	-	1.040	0.996	0.964	-	-

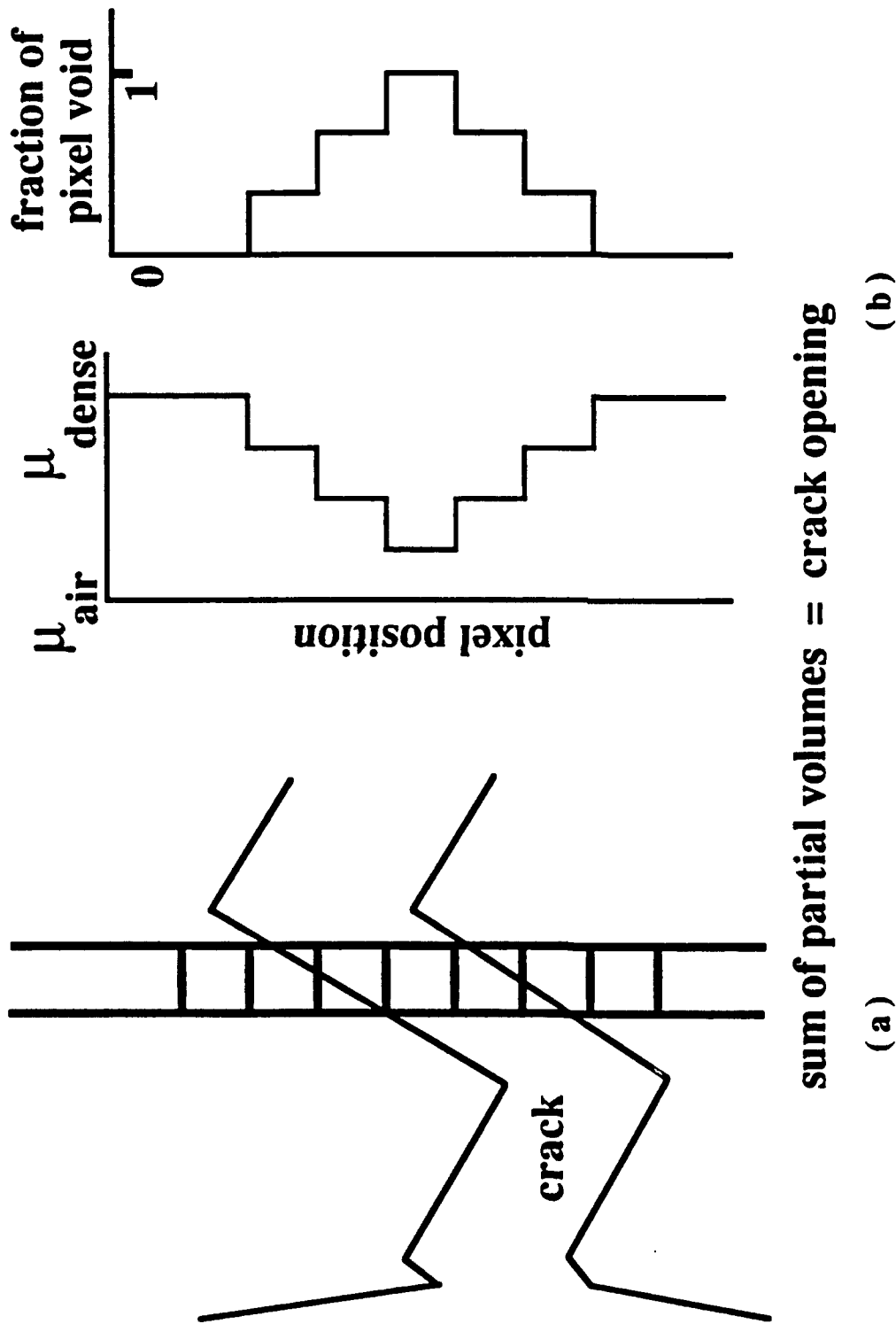


Figure 1 Measurement of crack opening as a function of position from XTM data. (a.) A column of voxels (parallel to the load axis) intersecting the crack. In the drawing, one voxel is completely within the crack, two voxels are predominantly within the crack and two voxels have only a small fraction of their volume within the crack. (b.) Schematic of the variation in linear attenuation of the pixels along the column shown in (a) and the corresponding fraction of voxels void.

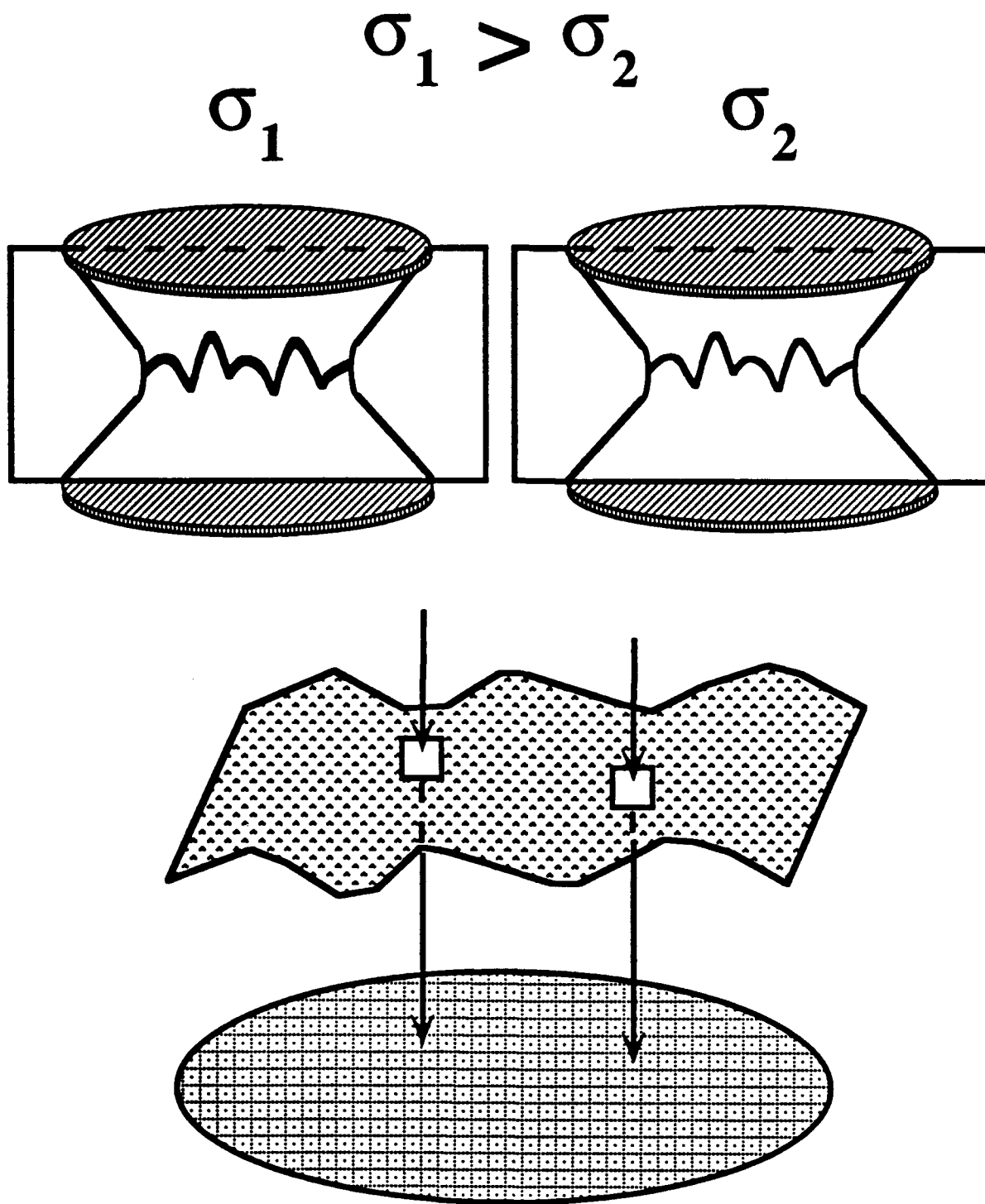


Figure 2 Illustration of projection of crack opening onto a single plain perpendicular to the load axis. The top figures show the crack's intersection with the surface of the sample. The drawing at the bottom of the page shows only the crack and the projection onto the plane perpendicular to the load axis.

MEASURED CRACK OPENINGS

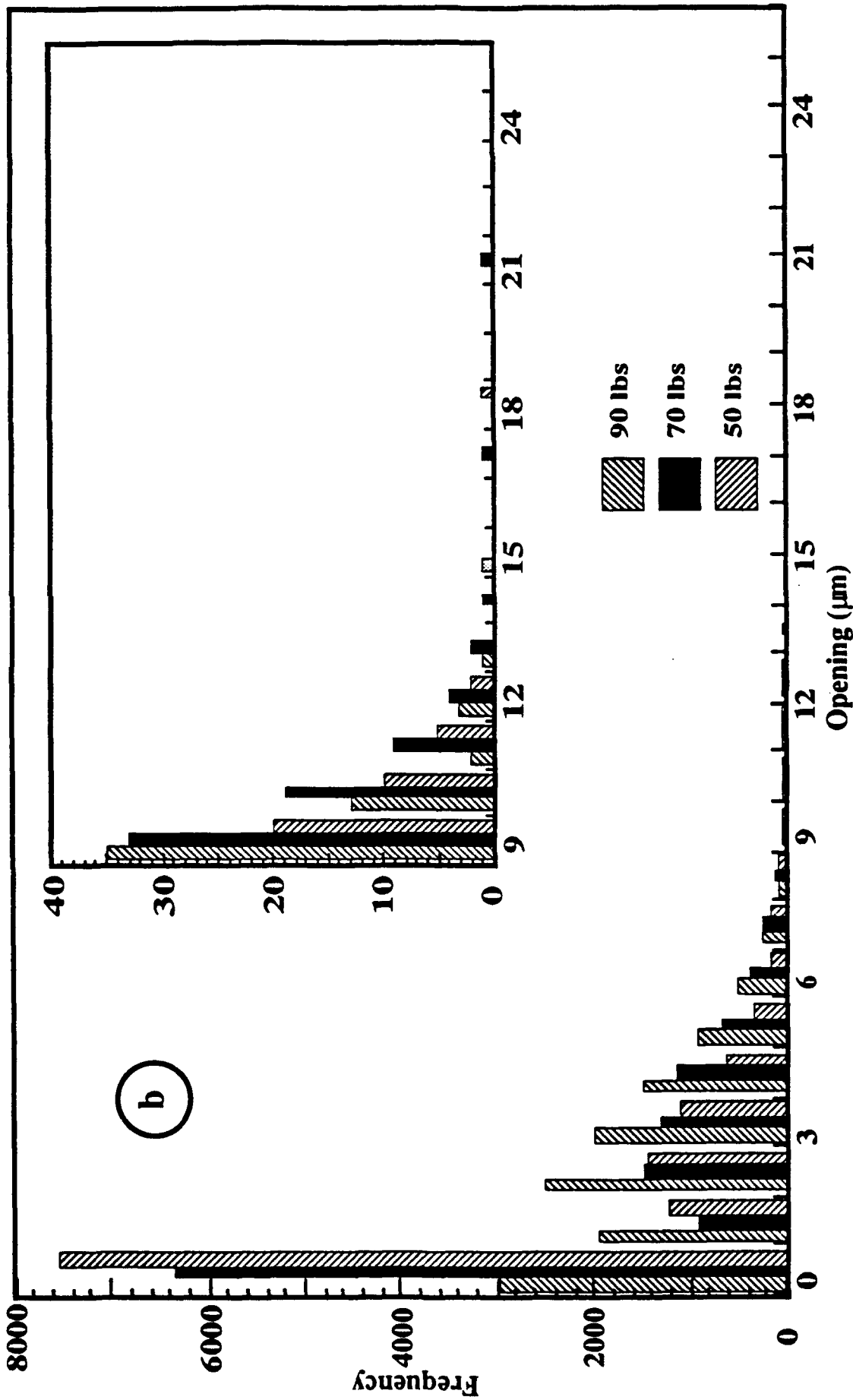


Figure 4 Histograms of crack opening measurements at: (a) 100, 80 and 60 lbs (45.4, 36.3 and 27.2 kg) and (b) 90, 70 and 50 lbs (40.9, 31.8 and 22.7 kg).

MEASURED CRACK OPENINGS

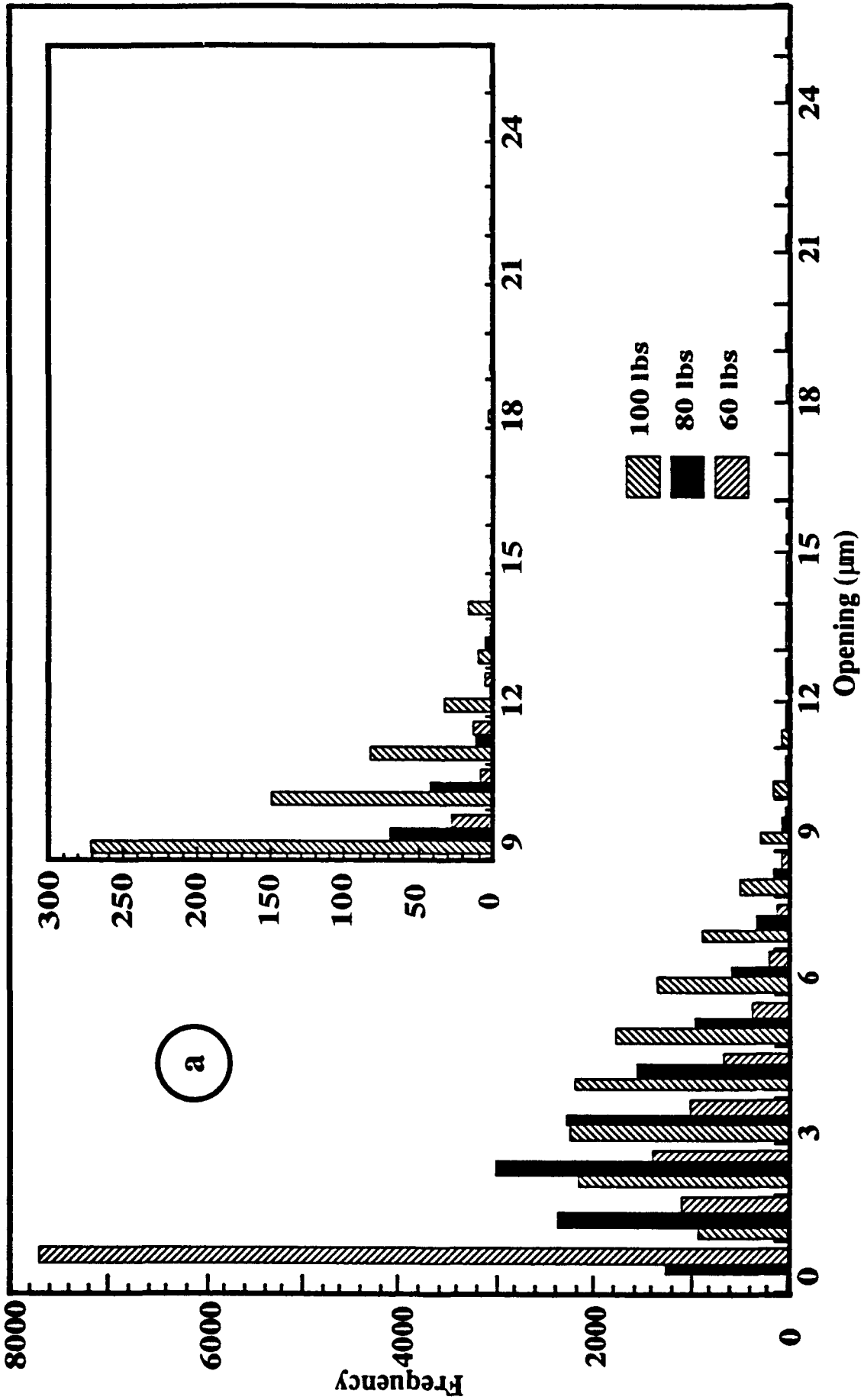


Figure 4 Histograms of crack opening measurements at : (a) 100, 80 and 60 lbs (45.4, 36.3 and 27.2 kg) and (b) 90, 70 and 50 lbs (40.9, 31.8 and 22.7 kg).

Comparison of K for Multi-Asperities

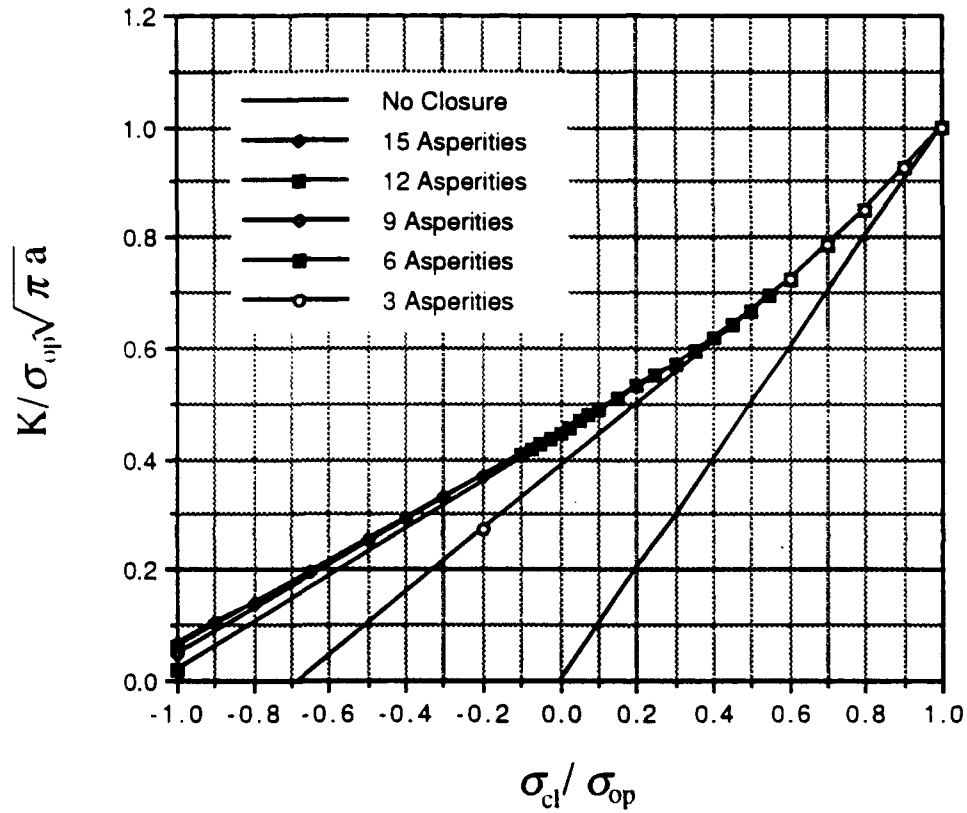


Fig. 5 Effects on closure stress intensity factor for a number of asperities distributed on fracture surface. Straight curves shown as a guide define items.

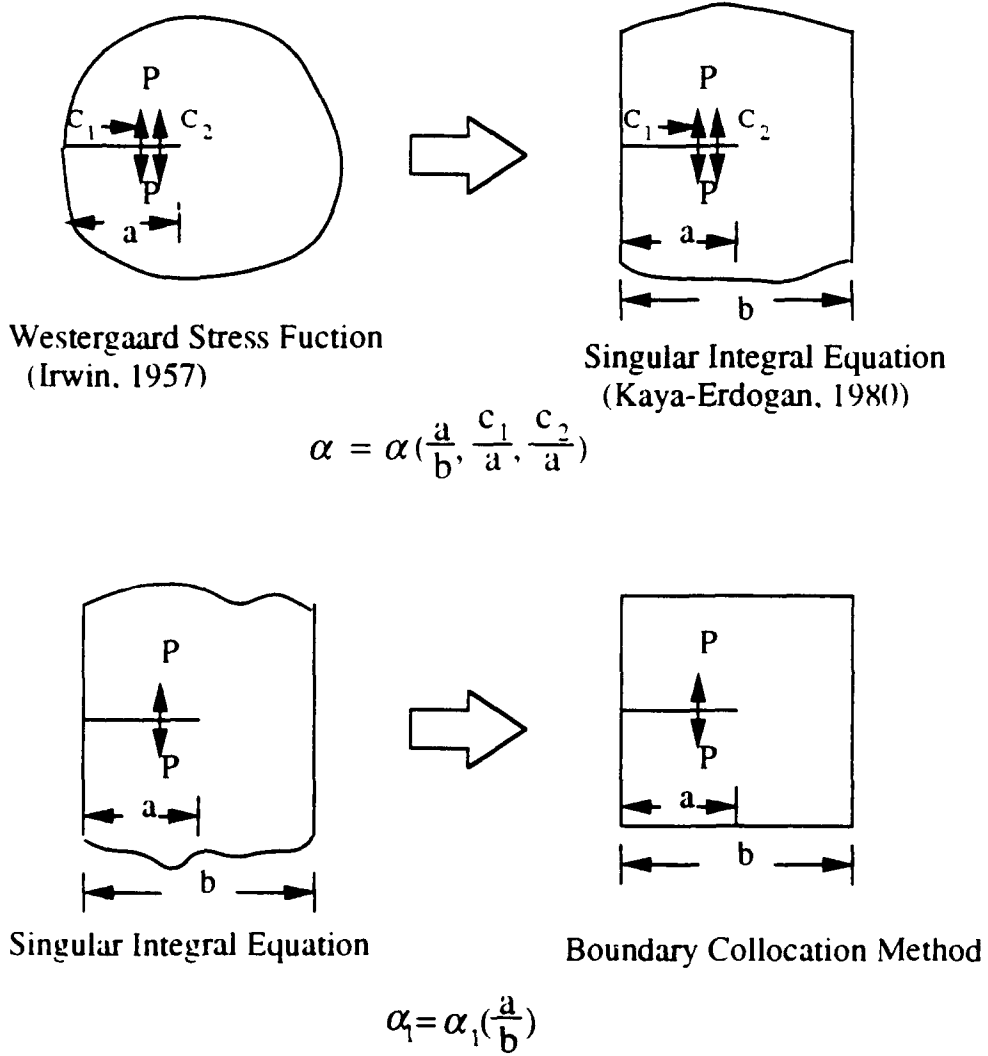
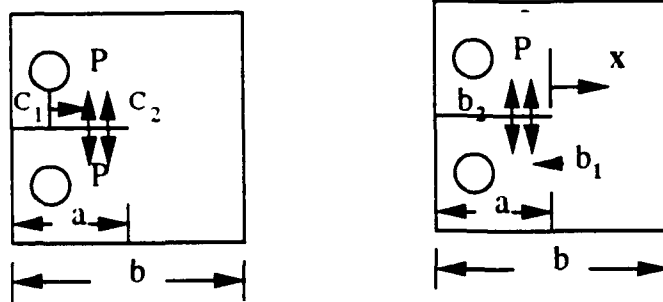


Fig. 6 Correction factors α and α_1 for CT specimen.



$$K_I = 2\sqrt{\frac{a}{\pi}} \frac{P}{B} \sqrt{2} \left(\sqrt{1 - \frac{c_1}{a}} - \sqrt{1 - \frac{c_2}{a}} \right) \alpha \alpha_1$$

$$\text{COD} = \frac{8a}{E\pi} \frac{P}{B} \left[\sqrt{\frac{|x|}{a}} \left(\sqrt{\frac{b_2}{a}} - \sqrt{\frac{b_1}{a}} \right) \right.$$

$$\left. + \frac{1}{2} \left(\frac{b_2}{a} + \frac{x}{a} \right) \log \left| \frac{\sqrt{|x|} + \sqrt{b_2}}{\sqrt{|x|} - \sqrt{b_2}} \right| - \frac{1}{2} \left(\frac{b_1}{a} + \frac{x}{a} \right) \log \left| \frac{\sqrt{|x|} + \sqrt{b_1}}{\sqrt{|x|} - \sqrt{b_1}} \right| \right] \alpha \alpha_1$$

Fig. 7 Stress intensity factor and COD for CT specimen.

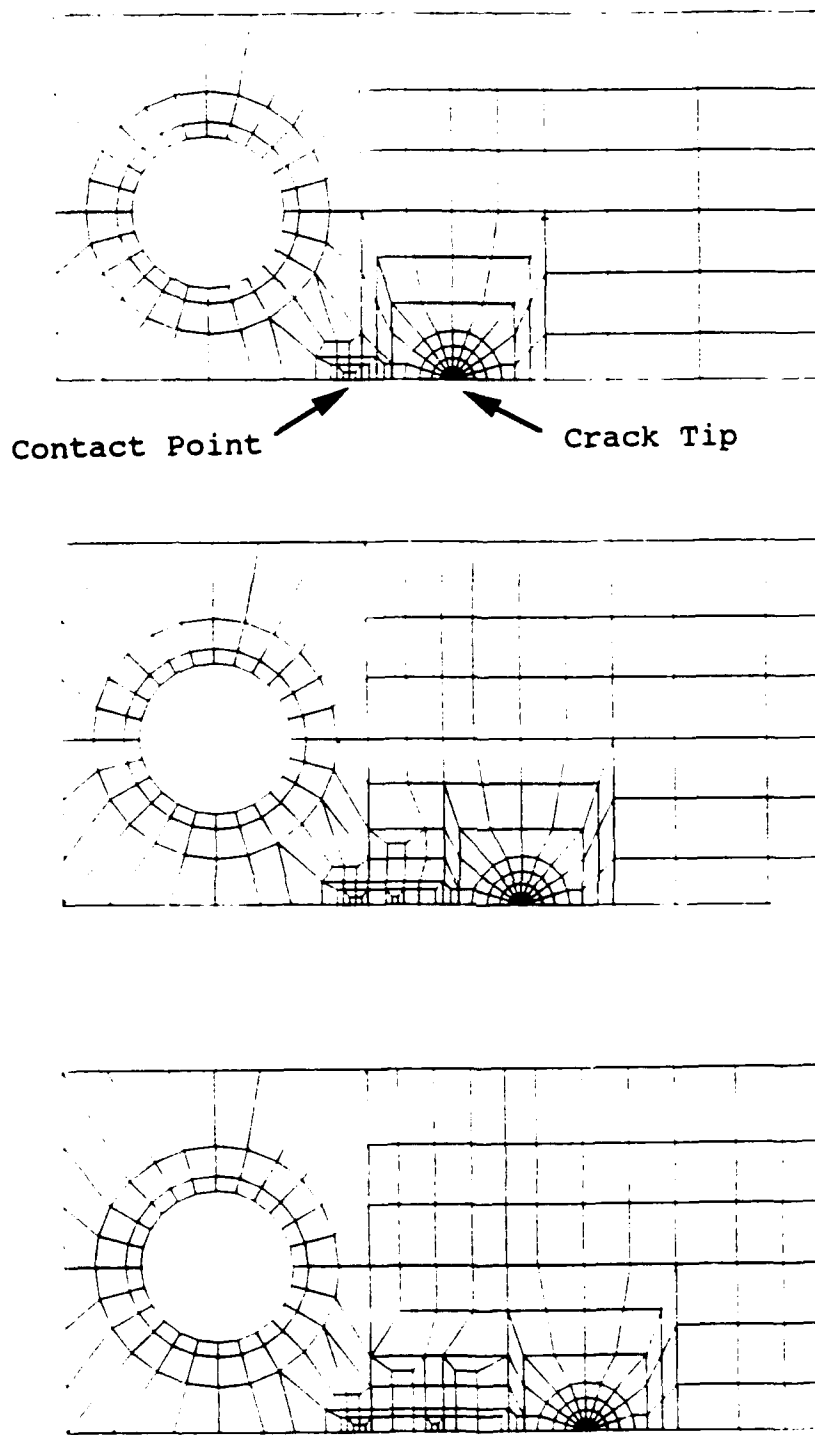


Fig. 8 Finite element meshes for calculating α_1 .

Correction Factor vs. c/a and a/b

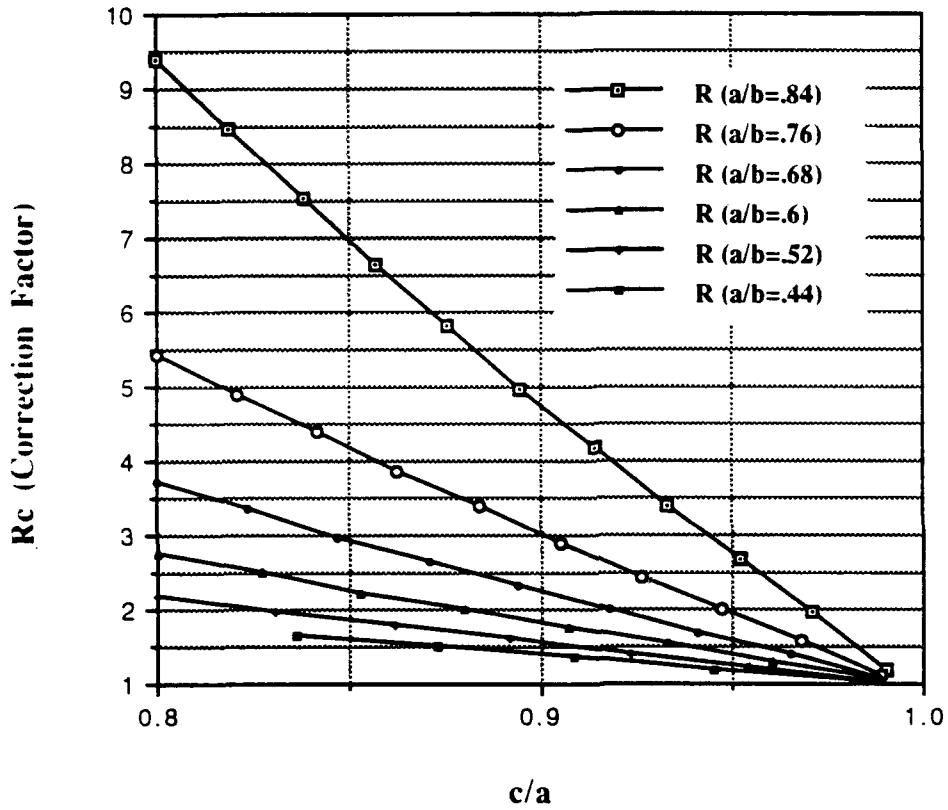


Fig. 9 Correction factor R vs contact point c/a for different values of dimensionless crack length a/b .

Fatigue Crack Propagation (Al-Li 2090)

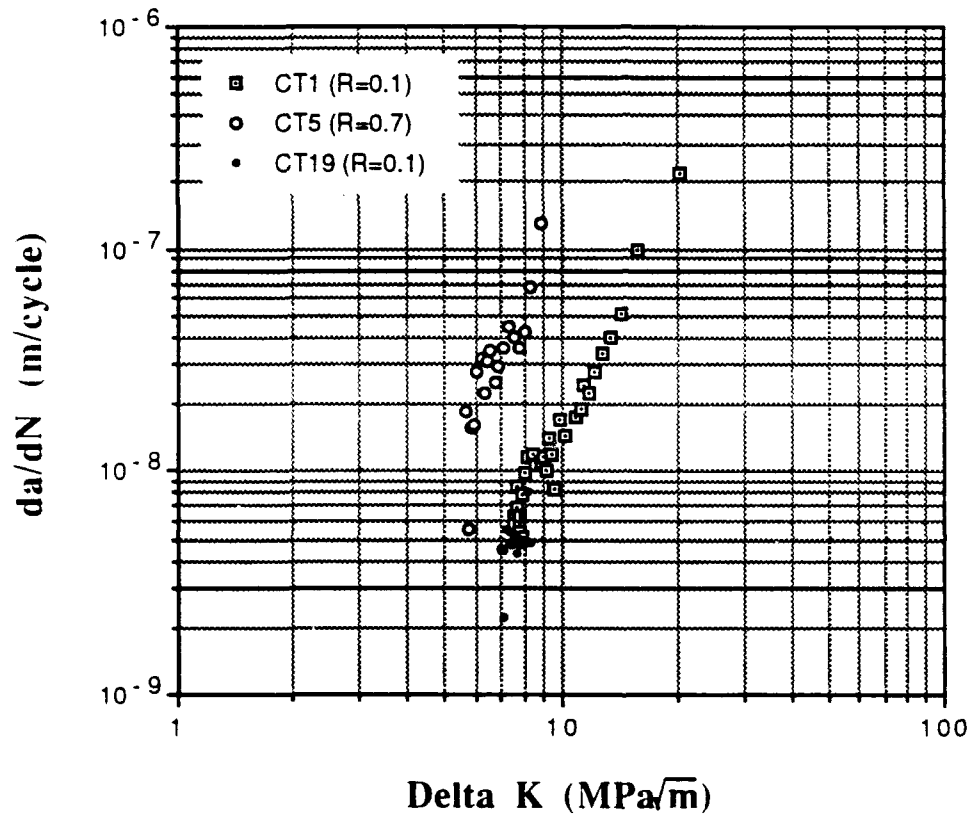


Fig. 10 Fatigue Crack Propagation Rate for Al-Li Alloy 2090.

FATIGUE CRACK PROPAGATION RATES OF Al-Li ALLOY 2090

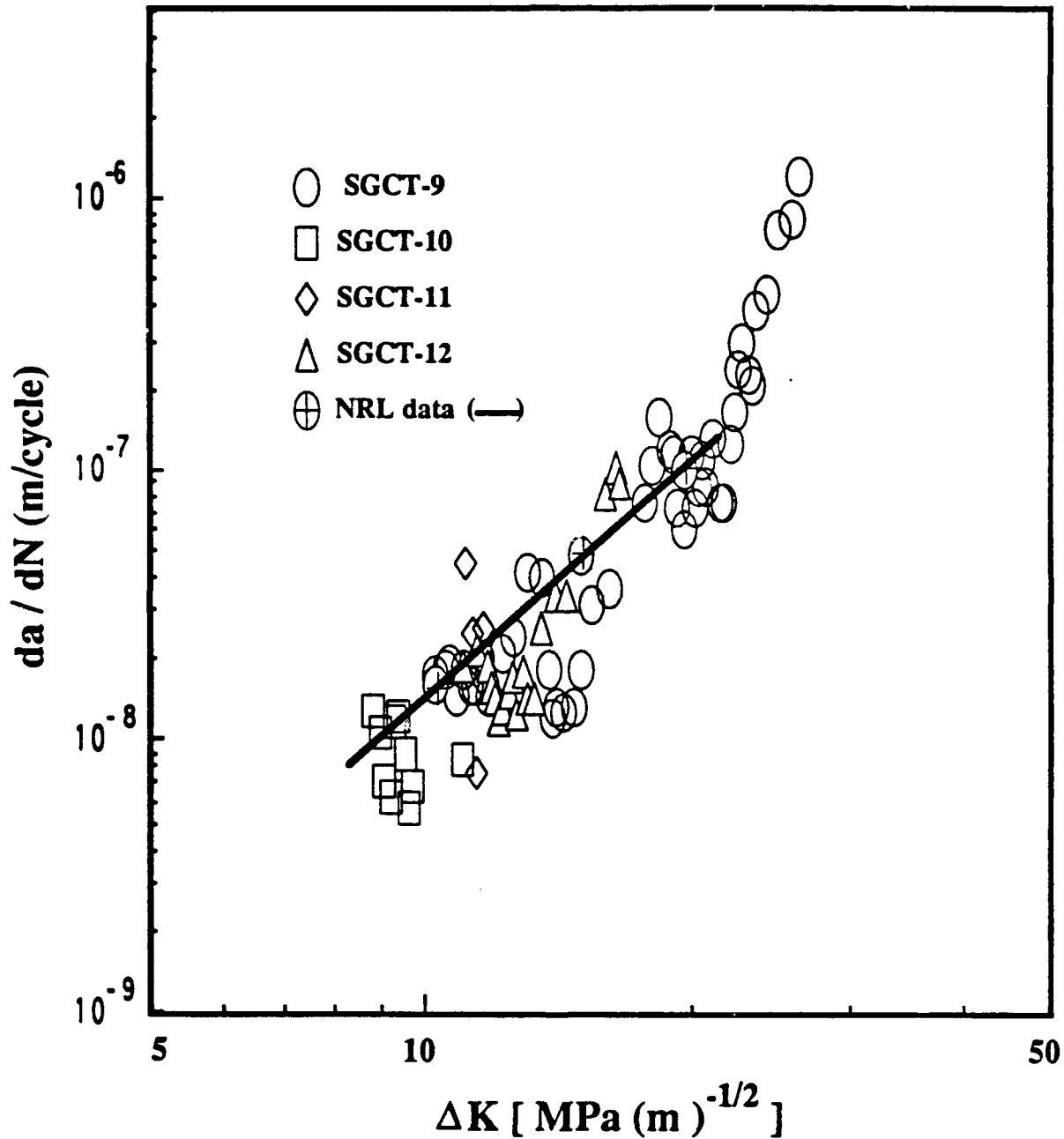


Figure 11 Crack propagation rates as a function of ΔK for SGCT samples 9-12 compared with data on a full size compact tension samples obtained on the same lot of material (L-T orientation) and under identical testing conditions at room temperature (haversine wave form, R: load ratio = 0.1 and frequency = 5 Hz) [8].

Ratio of Closure to Kmax (CT1,R=0.1)

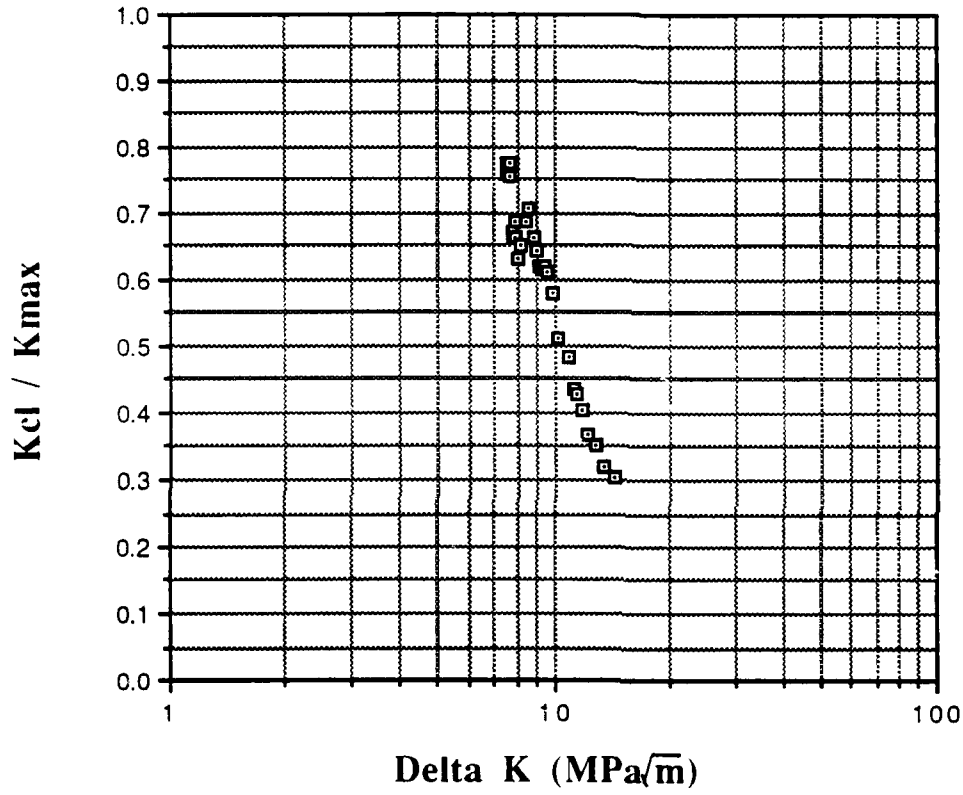


Fig. 12 Closure stress intensity factor vs. ΔK for sample CT1.

Comparison of Delta K and Keff (CT1,R=0.1)

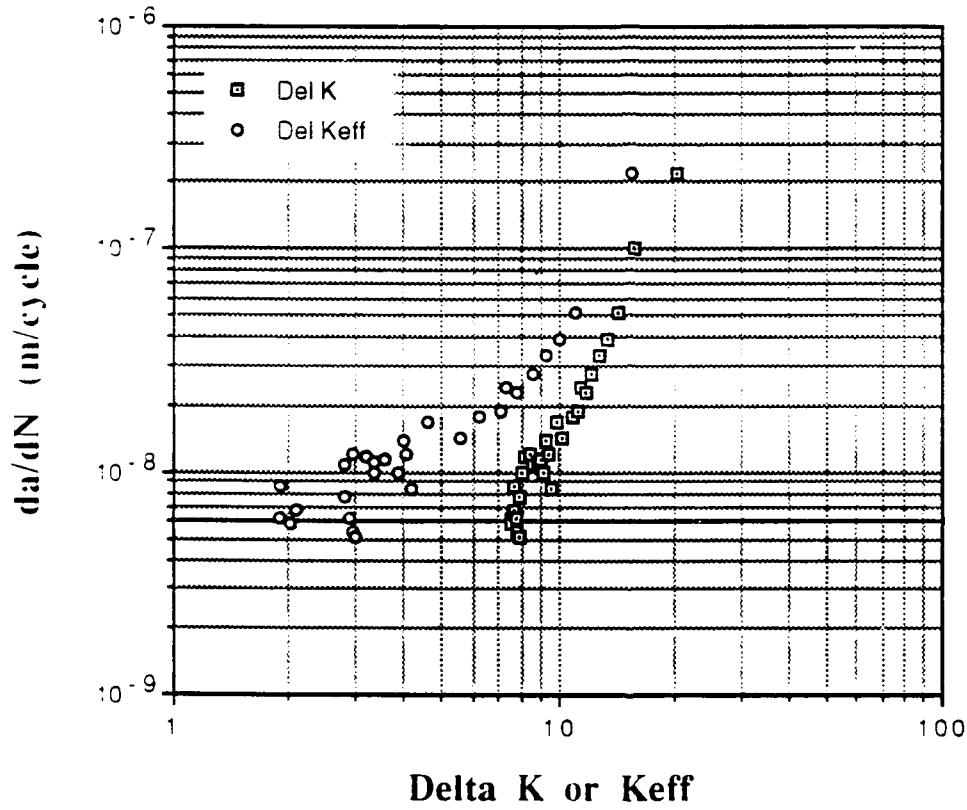


Fig. 13 Fatigue Crack Propagation Rate vs. ΔK_{eff}

da/dN vs. Crack Length for CT12

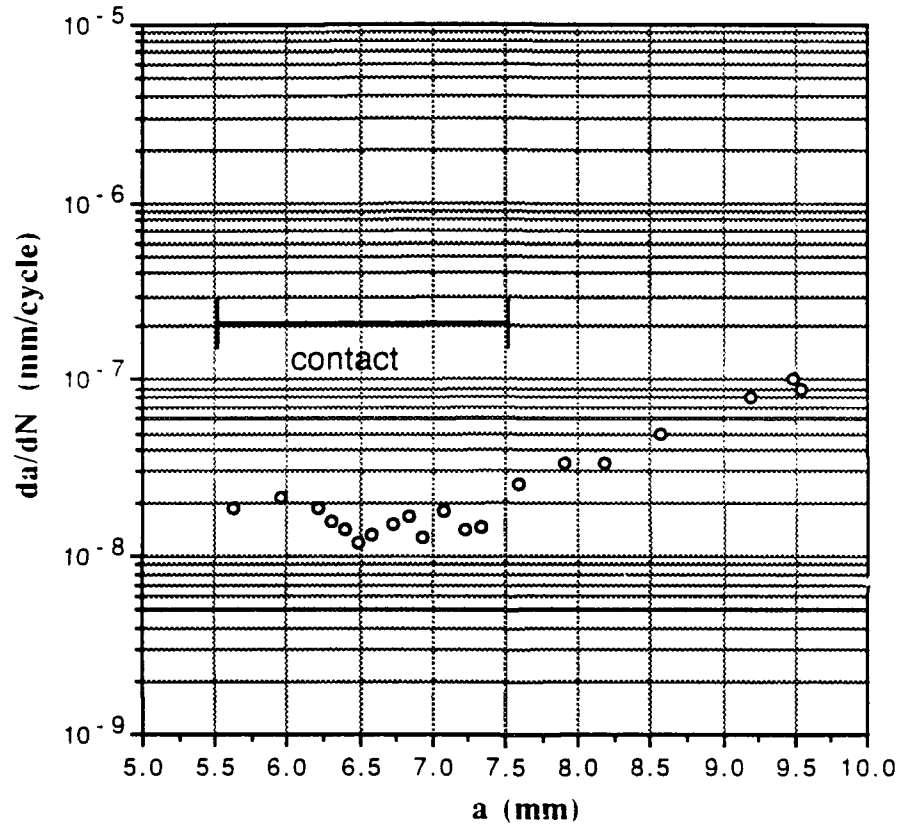


Fig. 14 Fatigue Crack Propagation Rate vs. Crack Length



Fig. 15 Fracture surface of Al-Li Alloy 2090 specimen. Crack propagation direction is from left to right.

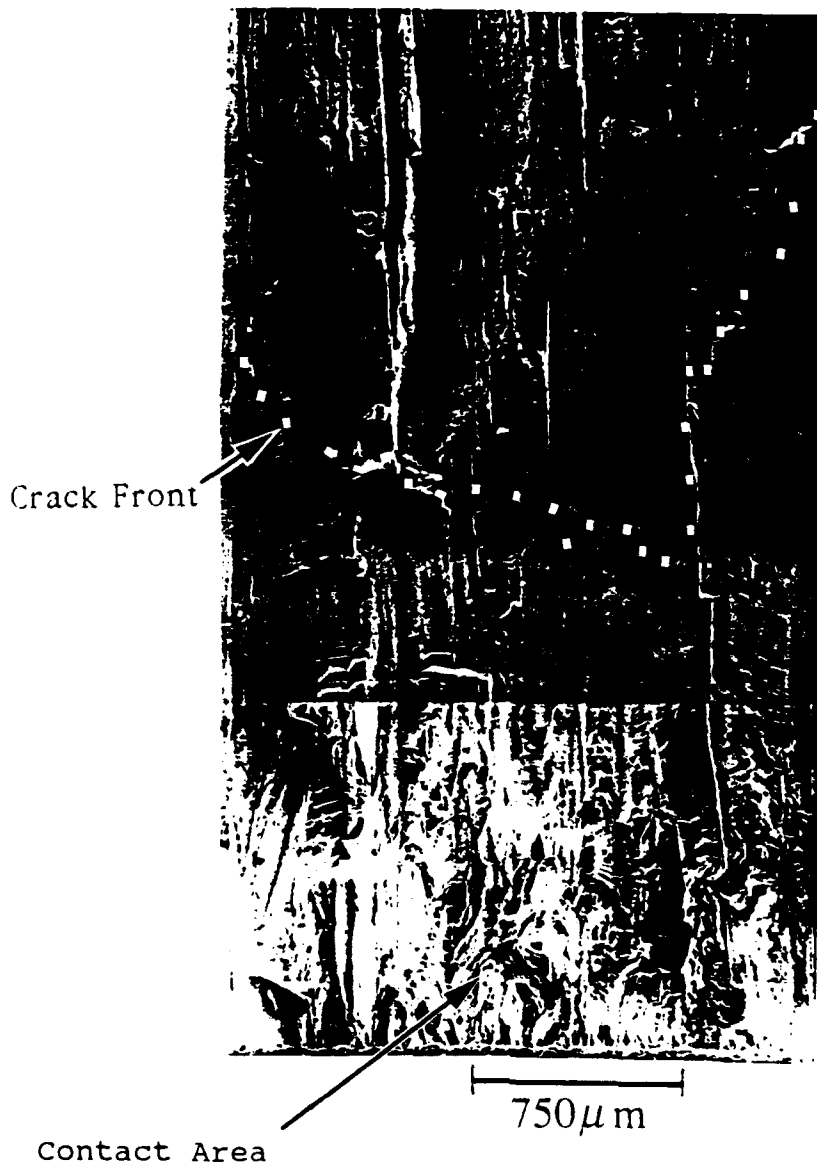


Fig. 16 Fracture surface of Al-Li alloy specimen showing a non-uniform crack front (white sequence) and the contact area. Crack propagation direction is from bottom to top.